STATE SPACE RECONSTRUCTION OF NON-LINEAR STALL-INDUCED OSCILLATORY AEROELASTIC MOTION

Flávio D. Marques, Eduardo M. Belo, Vilma A. Oliveira
Engineering School of São Carlos
University of São Paulo
São Carlos, Brazil

Keywords: *non-linear aeroelasticity, state space reconstruction, stall-induced motion, chaos*

Abstract

Stall-induced aeroelastic motion presents severe non-linear behavior. Mathematical models for predicting such phenomena are still not available for practical applications and they are not enough reliable to capture physical effects. Experimental data can provide suitable information to help the understanding of typical non-linear aeroelastic phenomena. Dynamical systems analysis techniques based on time series analysis can be adequately applied to non-linear aeroelasticity. When experimental data are available, the methods of state space reconstruction have been widely considered. This paper presents the state space reconstruction approach for the characterization of the stall-induced aeroelastic response non-linear behavior. A wind tunnel scaled wing model has been used to provide stall-induced aeroelastic responses. The wing model has been subjected to different airspeeds and dynamic incidence angle variations. The method of delays has been employed to identify an embedded attractor in the reconstructed state space from experimental aeroelastic response time series. To obtain the time delay value to manipulate the time series during reconstruction, the autocorrelation function analysis has been used. For the attractor embedding dimension calculation the correlation integral approach has been considered to obtain the conditions for invariants saturation. The reconstructed attractors can reveal typical non-linear structures associated to chaos or limit cycles.

1 Introduction

The treatment of aeroelastic phenomena with linear models have provided a reasonable amount of tools to the assessment and analysis of most of the adverse behaviour [1, 2]. Nonetheless, modern aviation has shown advances that lead to lighter and faster aircraft, thereby increasing the danger for severe aeroelastic problems. For instance, transonic flight is surrounded by a complex mixture of flows experiencing different speeds, aggravated by shock waves appearance. Aeroelastic phenomena associated to those compressibility effects introduce a great deal of non-linear effects, and can not be predicted with linear models [3]. Highly separated flows also lead to complex aeroelastic phenomena that are difficult to model [4].

Non-linear aeroelasticity research has recently become more relevant. Various approaches have been taken to model non-linear aeroelastic behaviour. In some cases the complex unsteady aerodynamics has been resolved with CFD methods [3], or by other methodologies to reduce the computational effort [4, 5]. However, the majority of non-linear aeroelastic models still need to be validated or checked. In this case, experimental data is of great importance, but it is not common to find significant non-linear aeroelastic data available.

Among the possible behaviour that a non-linear system presents one can assess are many equilibrium points, bifurcations, limit cycles,

chaos, etc. Bifurcations and limit cycles occur mainly in transonic aeroelastic responses or when introducing non-linear structural dynamics [6]. Moreover, chaotic motion almost certainly appears in highly separated flows, such as the case of dynamic stall [7].

The analysis of non-linear dynamical systems can be based on data from either a mathematical model or an experiment. A variety of mathematical tools have been available to explore and analyze such possible non-linear features, which can also be applied to aeroelastic problems [8]. Mathematical models for aeroelastic response associated to the dynamic stall behaviour or stall-induced motion are very hard to obtain. In this case, experimental or flight data seems to provide a more suitable basis for non-linear dynamical analysis. Experimental data furnishes a sequence of measurements that corresponds to a time series with the embedded system dynamics.

Typical dynamical systems responses can be assessed by means of reconstructing the state space from time series using the so-called *method of delays*. This technique has been shown to be robust enough to characterize non-linear dynamic systems, as well as to analyze chaotic behaviour. The fundamentals of this method have been introduced by Packard *et al.* [9] and Takens [10]. The method of delays uses delayed values of the time series to build a new coordinate system. This leads to the reconstruction of the state space for the observed dynamical system and any embedding attractor of interest in the true state space can be reconstructed. The main task of the method of delays is then to provide adequate values for the *time delays* and the so-called *embedding dimension* or *attractor dimension*. Several approaches to obtain the method of delays parameters have been investigated.

The purpose of this paper is to present techniques from the theory of time series analysis for the investigation of experimentally acquired non-linear aeroelastic phenomena. The characterization of the non-linear behaviour of stall-induced oscillations of an aeroelastic wing is achieved using the method of delays, leading to the state space reconstruction. An aeroelastic wing model has been constructed and tested in a wind tunnel. The wing model has been mounted on a turntable that allows variations in its incidence angle. Structural deformation is captured by means of strain gages, thereby providing information on the aeroelastic responses. The test cases correspond to aeroelastic response time series at specific strain gages points due to oscillatory motions of the turntable. A self-sustained oscillatory motion observed when the turntable is left free to move in the flow field, is also considered for analysis. The parameters for applying the method of delays are the time delay and the embedding (attractor) dimension. The autocorrelation function has been used to determine the time delays, while the correlation integral is used to obtain the embedding dimension. Evolutions of both power spectra and reconstructed state spaces, with respect to flow and motion parameters, are presented and discussed. This work represents a preliminary investigation towards the development of a concise framework for non-linear aeroelastic phenomena studies from experimentally acquired data.

2 State Space Reconstruction

Consider a dynamical system

$$\mathbf{x}(k+1) = \mathbf{F}(\mathbf{x}(k)) \tag{1}$$

where $\mathbf{x}$ and $\mathbf{F}$ are n-dimensional vectors. The embedding theorem attributed to Takens and Mañé [10, 11], established that if one is able to observe a single scalar quantity, say $h(\cdot)$, of some function $g(\mathbf{x}(k))$ then the geometric structure of the system dynamics can be unfolded from this set of scalar measurements $h(g(\mathbf{x}(k))$ in a space made out of new vector

$$\begin{aligned}\mathbf{y}_k \;=\; & [h(\mathbf{x}(k))\; h(g^1(\mathbf{x}(k)))\; h(g^2(\mathbf{x}(k)))\; \ldots \\ & h(g^{\mathrm{T}d-1}(\mathbf{x}(k)))]^{\mathrm{T}}\end{aligned} \tag{2}$$

which define motion in a d-dimensional space [12]. If d is large enough, for smooth functions $h(\cdot)$ and $g(\cdot)$ it is shown that many important properties of $\mathbf{x}(k)$ are reproduced in the new space given by $\mathbf{y}_k$ without ambiguity [13].

Let $s(k)$ denote the actual measured variable. If one choose

$$h(\cdot) = s(k)$$

and

$$g^i(\mathbf{x}(k)) = \mathbf{x}(k+T_i) = \mathbf{x}(t_0 + (k+T_i)\tau_s)$$

with τ_s being the sampling time, the new vector for $T_i = iT$ takes the form

$$\begin{aligned} \mathbf{y}_k &= [s(k)\ s(k+T)\ s(k+2T)\ \ldots \\ &\quad s(k+T(d-1)]^{\mathrm{T}}. \end{aligned} \tag{3}$$

The space constructed by using the vectors $\mathbf{y}_k$ is called the reconstructed space, the parameter T is called time delay and d the embedded dimension. According to the theory of state space reconstruction, the geometric structure of an attractor can be observed in the d-dimensional reconstructed space if $d \geq 2d_a + 1$, with d_a the dimension of the attractor of interest. The central issue in the reconstruction of the state space is the choice of the time lag $T\tau_s$ along with the dimension d.

The time lag $T\tau_s$ is usually chosen as the quarter of the period of the predominant frequency in the Fourier spectrum of the measured variable or equivalently T is found as the first zero of the linear autocorrelation function

$$C(T) = \sum_k [s(k) - \bar{s}][s(k+T) - \bar{s}] \tag{4}$$

where $\bar{s} = \frac{1}{N_0} \sum_{k=1}^{N_0} s(k)$ with N_0 is the total number of sampled points.

There are different methodologies to estimative the embedding dimension. When dynamical system responses are obtained from experiments, noise contamination is practically inevitable. The determination of the MOD parameters must follow specific procedures in order to guarantee proper state space reconstruction. The methodology considered here uses the saturation of system invariants, that is, the invariance properties of an attractor calculated from the reconstructed trajectory does not change by increasing d. To estimate d, the average fraction of the number of points on the attractor with interdistances less than r are calculated from the correlation integral $C(r)$ [8]:

$$C^d(r) = \frac{1}{M^2} \sum_{\substack{i,j=0 \\ i \neq j}}^{M} H(r - |\mathbf{y}_i - \mathbf{y}_j|) \tag{5}$$

where $M = N_0 - T(d-1)$ and $H(t)$ is the Heaviside function, that is:

$$H(u) = \begin{cases} 1 \text{ if } u \geq 0 \\ 0 \text{ if } u < 0 \end{cases}. \tag{6}$$

The $|.|$ is taken as the Euclidean distance

$$|\mathbf{y}_i - \mathbf{y}_j| = \sqrt{\sum_{k=1}^{d} (s_{i+T(k-1)} - s_{j+T(k-1)})^2}. \tag{7}$$

The correlation integral $C^d(r)$ is a function of r and the embedding dimension d. The slope of $\log_{10} C^d(r)$ versus $\log_{10} r$ is calculated as a function of d over a sufficient range for small interdistances r and the embedding dimension d is thus obtained when the slope becomes independent of d. The slope tends to saturate into a value called the correlation dimension.

3 Experimental Apparatus and Database

The aeroelastic wing comprises a wind tunnel model of an arbitrary straight rectangular semi-span wing. The wind tunnel facility presents a testing chamber with about $2m^2$ cross-section area, maximum flow speed in the testing chamber is $50\frac{m}{s}$. The wing model has been fixed to a turntable that allows incidence variation to the wing. The wing semi-span is $800mm$ and the chord is $290mm$.

The model main structure has been constructed using fiber glass and epoxy resin in the shape of a tapered plate. The taper ratio is of $1:1.67$, where the width at the wing root is $250mm$. To provide aerodynamic shape high density foam and wooden cover have been used. The NACA0012 airfoil from wing's root to tip has been used. In order to minimize as much as possible the effects of the skin to the wing structure

stiffness, both foam and wooden shell have been segmented at each 100*mm* spanwise.

Figure 1 illustrates the experimental apparatus with indications of the strain gages locations inside the wing model.

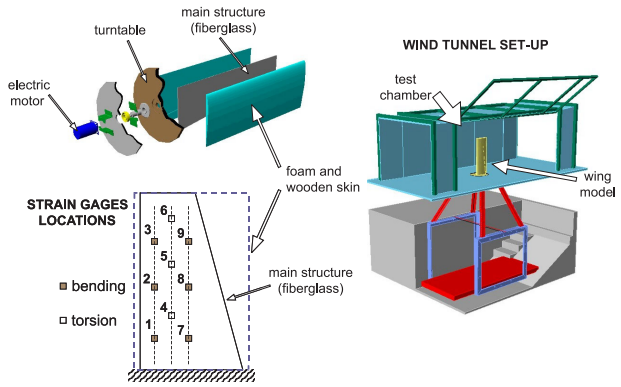

Fig. 1 Experimental set-up and strain gages locations.

Incidence motion is achieved with an electrical motor mounted beneath the turntable. The motor actions are controlled by software integrated to the acquisition system. Strain gages have been fixed to the plate surface to furnish proper measurement of the dynamic response of the wing main structure. The strain gages have been distributed along three lines spanwise. The first and last lines present three strain gages each, all to capture bending motions. The intermediate line presents three strain gages for torsional motion.

4 Aeroelastic State Space Reconstruction

The experiments consist in applying prescribed turntable motion with the acquisition of the aeroelastic response from strain gages signals. Prescribed turntable motions correspond to oscillatory and random ones, and they have been also carried out at different airspeeds (from 9 to 16.5 $\frac{m}{s}$, approximately). Oscillatory motions have been run at relatively low amplitude values (maximum of 5.5°), but such oscillations have been considered around two average angles, that is, zero and 9.5°. For the cases where the average oscillatory angle is about 9.5°, highly unsteady separated flow is occurring. These cases furnish an adequate database for non-linear phenomena investigation. Figure 2 presents a typical aeroelastic response time-history that has been measured during an oscillatory test case. The case correspond to an oscillatory one, where the airspeed is 16.89 $\frac{m}{s}$, reduced frequency is $k = 0.1374$, average angle of incidence is $\alpha_m = 9.5°$ and motion amplitude equals to 5.5°. One can observe the existence of complex aeroelastic response that can be inferred as the result of highly separated flow.

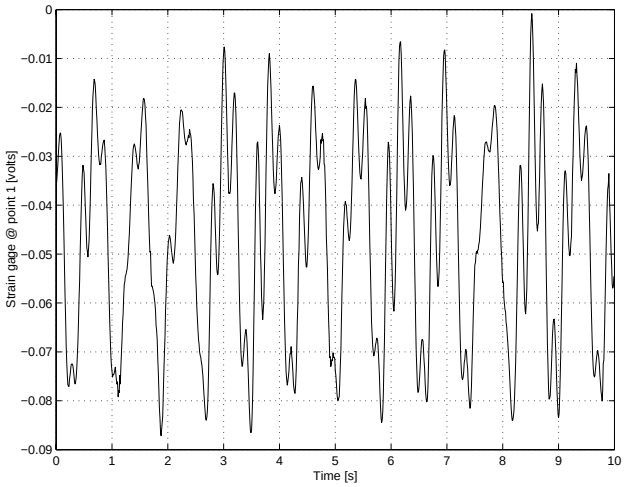

Fig. 2 Aeroelastic response time history (oscillatory turntable).

The randomly generated motions follow the same strategy. Tests have been also proceeded for static turntable at different incidences and for free turntable at a range of flow speeds. For the last one, it has been observed a peculiar self-sustained oscillatory motion at higher angles of attack. The aeroelastic responses associated to this free turntable condition is also examined in this paper.

The techniques for assessing the time delay and embedding (attractor) dimension have been used to provide the basic parameters for state space reconstruction. Figure 3 shows the time delay determination by means of the autocorrelation function. The time delay is taking where the autocorrelation function becomes zero. Figure 4 illustrates the embedding dimension determination via the analysis of the correlation

integral and its saturation as the dimension increases. Saturation can be observed when the curves of $\log_{10} C^d(r)$ versus $\log_{10} r$ for each dimension present a similarity in their slopes.

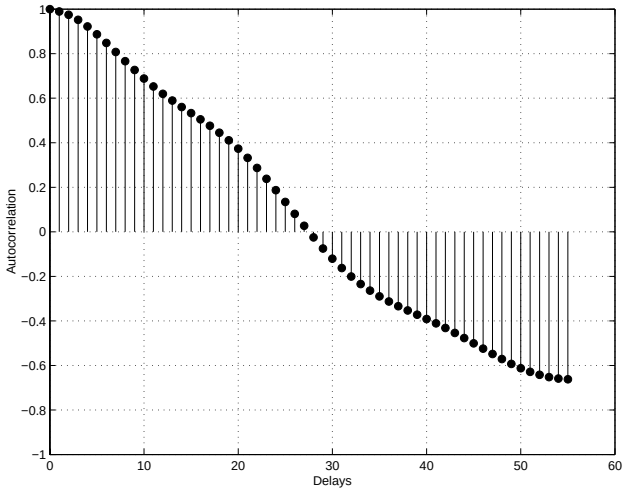

Fig. 3 Autocorrelation function and time delay (T) determination.

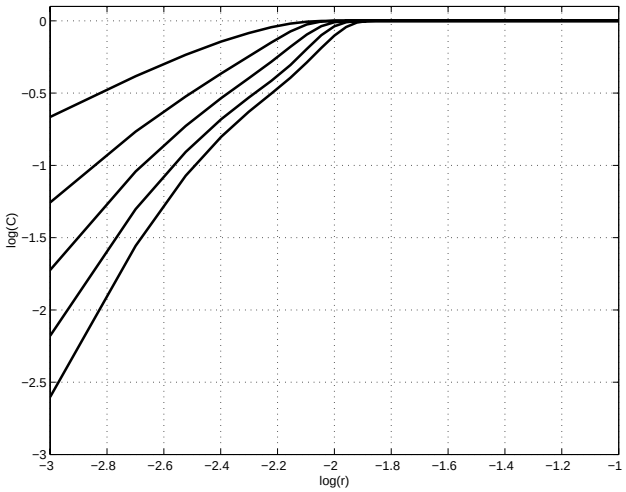

Fig. 4 Determination of embedding (or attractor) dimension (d).

State space reconstruction has been achieved for two different motion cases. Firstly, aeroelastic responses due to oscillatory turntable motion are considered, and, then, stall-induced aeroelastic responses when the turntable is free to move are also considered.

4.1 Oscillatory turntable

Aeroelastic responses associated to the strain gages at points 1 and 4 (*cf.* Figure 1) are assumed. These strain gages are used to measure bending and torsional displacements, respectively, thereby allowing to access time series of important components of the wing aeroelastic behavior.

Bending measurements have been acquired at three different flow speeds and for different oscillatory frequencies. The outcome of time delay determination for those cases are summarized in the Table 1, where U_∞ is the free-stream velocity, ω is the oscillatory frequency, and k is the reduced frequency. The resulting time delays have shown a direct relation to the oscillatory frequencies, but no relation to the free-stream velocities. The embedding dimension is found to be 3, which leads to the reconstructed state space vectors as $\mathbf{y}_k = [x(k)\ x(k+T)\ x(k+2T)]^{\mathrm{T}}$ (attractor embedded in R^3).

Table 1 Parameters of bending measurements for oscillating turntable.

Case	$U_\infty(\frac{m}{s})$	$\omega(Hz)$	k	time delay
1	11.19	0.47	0.0778	50
2		1.27	0.2078	20
3	13.58	0.47	0.0641	49
4		1.27	0.1709	20
5		1.59	0.2136	9
6	16.89	1.27	0.1374	20
7		2.07	0.2233	8

For a turntable oscillatory frequency of $1.27Hz$ and varying the free-stream velocity, the power spectrum evolution presents a dominant fundamental frequency and its super-harmonics as shown in Figure 5. When oscillatory frequencies are varied for the same free-stream velocity, the power spectrum presents evolution different patterns of super-harmonics as reduced frequency increases. Figure 6 illustrates the power spectrum evolution for varying reduced frequency. From Figures 5 and 6 one can infer

that super-harmonic frequencies pattern is basically the same for free-stream velocity variation, while increasing reduced frequencies reveals a more complex super-harmonic appearance mechanism.

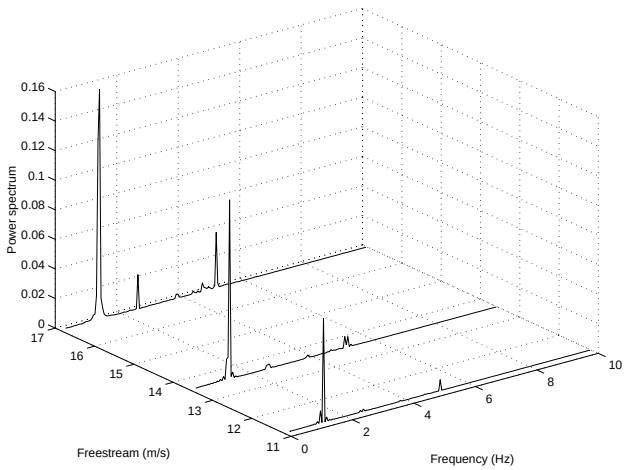

Fig. 5 Power spectrum evolution of bending measurements with free-stream velocity variation (cases 2, 4 and 6 from Table 1).

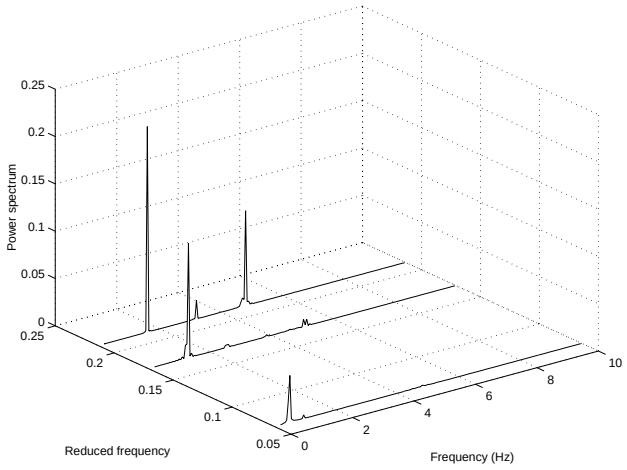

Fig. 6 Power spectrum evolution of bending measurements with reduced frequency variation (cases 3 to 5 from Table 1).

State space reconstructions for cases when the free-stream velocities and reduced frequencies vary are, respectively, presented in Figures 7 and 8. Here the evolution of the reconstructions are shown in terms for the attractor R^2 projections $\mathbf{y}_k = [x(k)\ x(k+T)]^{\mathrm{T}}$, in order to make it easy to observe the phenomena. Figure 7 presents the case where the reconstructed spaces evolve for increasing free-stream velocities and fixed oscillatory frequency. It corresponds to the same power spectrum evolution shown in Figure 5. As in the spectrum evolution, the reconstructed state spaces present similar pattern as the velocity increases, differing only on the displacement amplitudes. However, in Figure 8 the evolution of the reconstructed state spaces for a fixed free-stream velocity shows complex patterns as reduced frequency increases. Such complexity in both shape and amplitude of the orbits may be connected to strong non-linear phenomena such as chaos or bifurcations. Further investigations using methodologies to identify chaotic structures shall be develop.

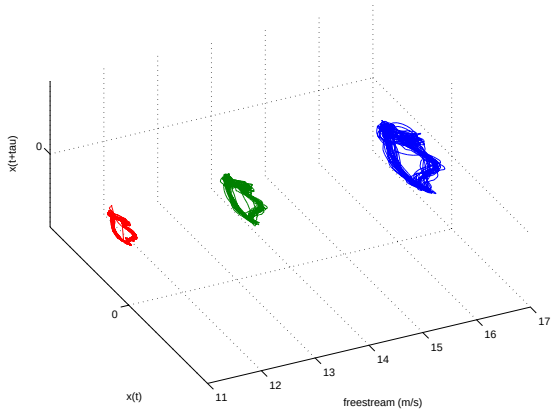

Fig. 7 Reconstructed state spaces of bending measurements with free-stream velocity variation (cases 2, 4 and 6 from Table 1).

For torsional measurements (from strain gage at point 4 in Figure 1), the same procedure adopted in the case of bending measurements is considered. Table 2 presents the time delays that have been obtained for the wing torsion measurement time series, where U_∞ is the free-stream velocity, ω is the oscillatory frequency, and k is the reduced frequency. Here, the time delay values have also shown a coherence with respect to the oscillatory frequency.

Figures 9 and 10 present the power spectrum evolution of torsional measurement time series for varying free-stream velocity and reduced fre-

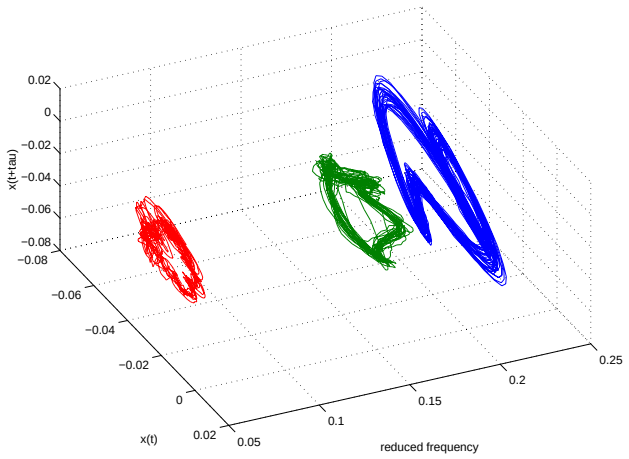

Fig. 8 Reconstructed state spaces for bending measurements with reduced frequency variation (cases 3 to 5 from Table 1).

quency cases, respectively. Similarly to the bending measurements, here the power spectra reveal complex frequency content when reduced frequencies increase (*cf.* Figure 10).

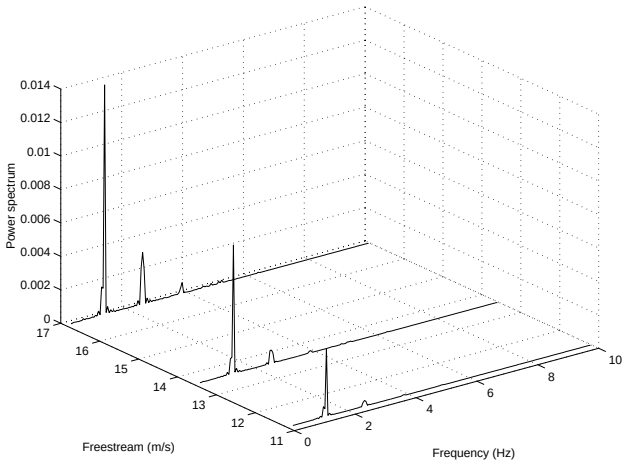

Fig. 9 Power spectrum evolution of torsional measurements with free-stream velocity variation (cases 2, 4 and 6 from Table 2).

Figures 11 and 12 present the reconstructed state spaces for cases when the free-stream velocities and reduced frequencies vary, respectively. The evolution of the reconstructions are shown in terms for the projections $\mathbf{y}_k = [x(k)\ x(k+T)]^{\mathrm{T}}$, as in the bending measurement time series analysis. The results have shown strong influence from noisy data, however the structure of each trajectory can be observed. Differently of the bending measurement time series, in these cases both evolution in free-stream velocity and reduced frequency have followed a characteristic pattern. The only parameter that effectively rises from the reconstructed spaces is the motion amplitude.

Table 2 Parameters of torsional measurements for oscillating turntable.

Case	$U_\infty(\frac{m}{s})$	$\omega(Hz)$	k	time delay
1	11.12	0.47	0.0783	40
2		1.27	0.2087	17
3	13.60	0.47	0.0640	39
4		1.27	0.1706	17
5		1.59	0.2132	11
6	16.35	1.27	0.1370	14
7		2.07	0.2227	9

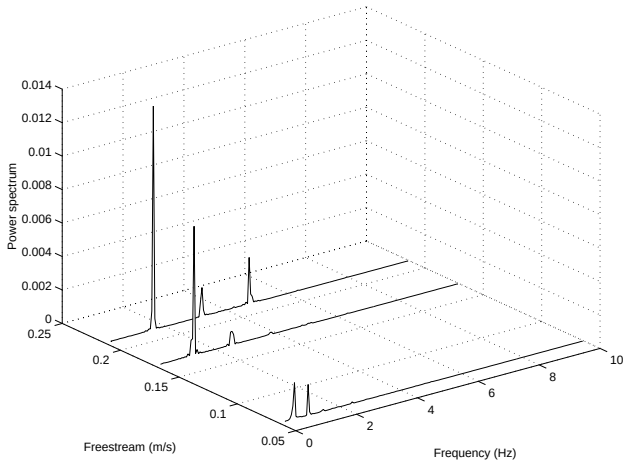

Fig. 10 Power spectrum evolution of torsional measurements with reduced frequency variation (cases 3 to 5 from Table 2).

4.2 Free turntable

When the turntable is left free, the aerodynamic forces and other flow effects are the responsible for the wing motion. It has been observed a peculiar self-sustained oscillatory motion of the wing, typical of a limit cycle. The oscillatory motion has kept the amplitude confined in between 4.0° to 14.0° turntable incidence angle. In these cases

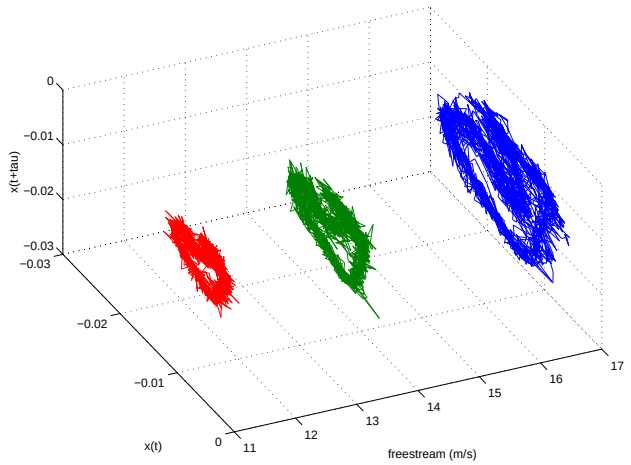

Fig. 11 Reconstructed state spaces of torsional measurements with free-stream velocity variation (cases 2, 4 and 6 from Table 2).

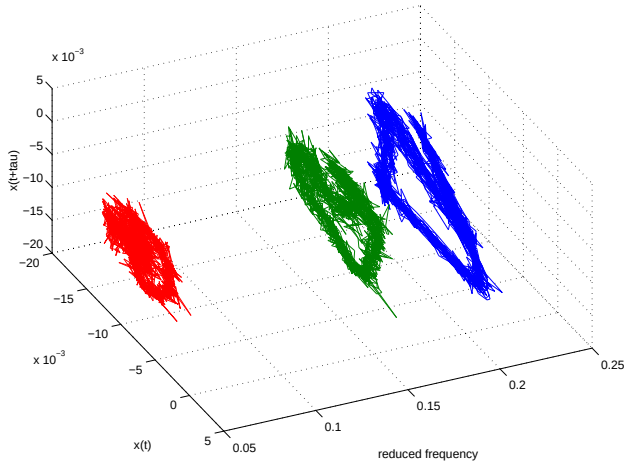

Fig. 12 Reconstructed state spaces for torsional measurements with reduced frequency variation (cases 3 to 5 from Table 2).

the stall has induced a deep break to the increasing pitching moment that builds up for the free wing motion immerse into the flow. Both incidence angle and frequencies increase as flow speed also increases.

The torsional measurement time series, that has been acquired from the strain gage at the point 4 (*cf.* in Figure 1), has been used to reconstruct the state space. The experiments have been carried out for six different free-stream velocities and the resulting time delays for these cases are summarized in the Table 3, where U_∞ is the free-stream velocity. Similarly to the prescribed oscillatory turntable motion cases, here the embedding dimension is found to be 3, which also leads to the reconstructed vectors as $\mathbf{y}_k = [x(k)\ x(k+T)\ x(k+2T)]^{\mathrm{T}}$.

Table 3 Parameters for free turntable.

Case	$U_\infty(\frac{m}{s})$	time delay
1	9.42	27
2	11.46	24
3	13.49	22
4	14.29	21
5	15.13	20
6	16.75	18

Figure 13 presents the evolution of the power spectrum for the case of free turntable with respect to the flow velocity. The spectra show a dominant fundamental frequency and their superharmonics.

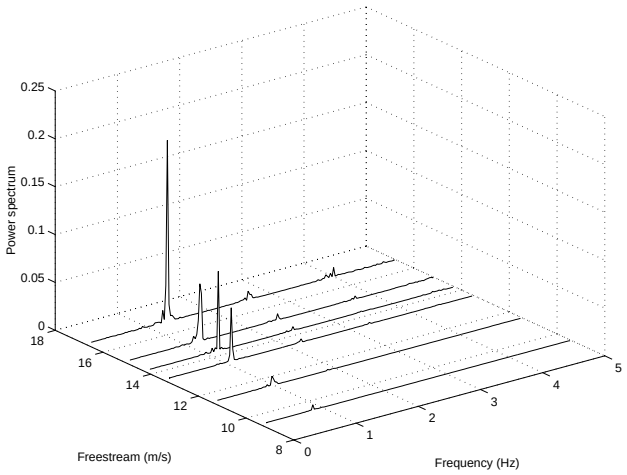

Fig. 13 Power spectrum evolution with respect to the free-stream velocity for free turntable case.

Figure 14 shows the evolution in terms of free-stream velocity of the reconstructed state spaces. Periodic motion is evident from the obtained trajectories. The bouncing phenomenon is also observed in these cases, which characterizes the existence of a resonance mode. The effect of stall inducing the breakdown in pitching moment may be the reason for such phenomenon. The re-

constructed state spaces depict a closed orbit that corresponds to a limit cycle.

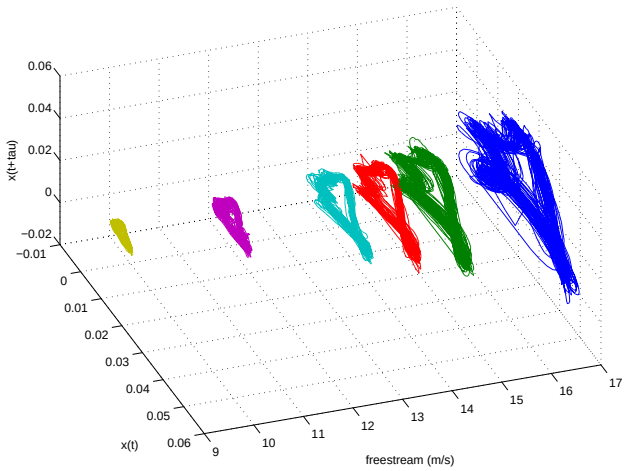

Fig. 14 Evolution with respect to the free-stream velocity of reconstructed state spaces for free turntable cases.

5 Concluding Remarks

Techniques from the theory of time series analysis, in the context of non-linear systems, is used in this paper to investigate experimentally acquired non-linear aeroelastic phenomena. An aeroelastic wing model has been tested in wind tunnel. Aeroelastic responses have been obtained from strain gages outputs. The wing is mounted on a turntable that allows variations to the incidence angle. The aeroelastic time series are related to oscillatory and free turntable motions. The aeroelastic responses studied in this paper are influenced by highly separated flow fields. The method of delays is employed and for the oscillatory turntable motion a complex evolution of the reconstructed state space is observed when reduced frequency varies for the same freestream velocity. It is possible to infer that bifurcation and chaotic behaviour are related to the aeroelastic system. The employment of techniques to assess the Lyapunov exponents may ensure the existance, or not, of a chaotic behavior. It has been observed that when the turntable is left free in the aerodynamic flow, a self-sustained oscillation happens. In this case, the existence of the bouncing phenomenon, characterizing a resonance mode, is observed. The reconstructed attractors depict a closed orbit corresponding to a limit cycle.

Acknowledgements

The authors acknowledge the financial support of the São Paulo State Research Agency - FAPESP (grant 97/13323-8) and the Brazilian Federal Research Council - CNPq (grant 520356/00-4) during the tenure of this research work.

References

[1] P. P. Friedmann. The the renaissance of aeroelasticity and its future. In *Proceedings of the International Forum on Aeroelasticity and Structural Dynamics, CEAS 97*, volume 1, pages 19–49, Roma, Itália, 17-20 Junho 1997.

[2] I. E. Garrick. Aeroelasticity - frontiers and beyond. *Journal of Aircraft*, 13(9):641–657, 1976.

[3] J. W. Edwards. Computational aeroelasticity. In A. K. Noor and S. L. Vemuri, editors, *Structural Dynamics and Aeroelasticity*, volume 5 of *Flight-Vehicle Materials, Structures, and Dynamics - Assessment and Future Directions*, pages 393–436. ASME, 1993.

[4] J. G. Leishman and T. S. Beddoes. A semi-empirical model for dynamic stall. *Journal of the American Helicopter Society*, 34:3–17, 1989.

[5] F. D. Marques. *Multi-Layer Functional Approximation of Non-Linear Unsteady Aerodynamic Response*. PhD thesis, University of Glasgow, Glasgow, UK, 1997.

[6] H. Alighanbari and S. J. Price. The post-hopf-bifurcation response of an airfoil in incompressible two-dimensional flow. *Nonlinear Dynamics*, 10:381–400, 1996.

[7] L. E. Ericsson and J. P. Reding. Dynamic stall at high frequency an large amplitude. *Journal of Aircraft*, 17:136–142, 1980.

[8] A. H. Nayfeh and B. Balachandran. *Applied Nonlinear Dynamics*. John Wiley & Sons, New York, 1995.

[9] N. H. Packard, J. D. Farmer, J. P. Crutchfield,

and R. S. Shaw. Geometry of time series. *Physical Review Letters*, 45(9):712–716, 1980.

[10] F. Takens. Detecting strange attractors in turbulence. In D. Hand and L.S. Young, editors, *Dynamical Systems and Turbulence*, pages 366–381. Springer, 1981.

[11] R. Mañé. On the dimension of compact invariant sets of certain nonlinear maps. In D. Hand and L.S. Young, editors, *Dynamical Systems and Turbulence*, pages 230–242. Springer, 1981.

[12] H. D. I. Abarbanel. *Analysis of Observed Chaotic Data*. Springer-Verlag, New York, 1996.

[13] T. Sauer, J. A Yorke, and M. Casdalgi. Embedology. *Journal of Statistical Physics*, 65:579–616, 1991.